# Slow Inactivation in Human Cardiac Sodium Channels

J. E. Richmond, D. E. Featherstone, H. A. Hartmann, and P. C. Ruben
Department of Biology, Utah State University, Logan, Utah 84322-5305 USA

ABSTRACT The available pool of sodium channels, and thus cell excitability, is regulated by both fast and slow inactivation. In cardiac tissue, the requirement for sustained firing of long-duration action potentials suggests that slow inactivation in cardiac sodium channels may differ from slow inactivation in skeletal muscle sodium channels. To test this hypothesis, we used the macropatch technique to characterize slow inactivation in human cardiac sodium channels heterologously expressed in *Xenopus* oocytes. Slow inactivation was isolated from fast inactivation kinetically (by selectively recovering channels from fast inactivation before measurement of slow inactivation) and structurally (by modification of fast inactivation by mutation of IFM1488QQQ). Time constants of slow inactivation in cardiac sodium channels were larger than previously reported for skeletal muscle sodium channels. In addition, steady-state slow inactivation was only 40% complete in cardiac sodium channels, compared to 80% in skeletal muscle channels. These results suggest that cardiac sodium channel slow inactivation is adapted for the sustained depolarizations found in normally functioning cardiac tissue. Complete slow inactivation in the fast inactivation modified IFM1488QQQ cardiac channel mutant suggests that this impairment of slow inactivation may result from an interaction between fast and slow inactivation.

## INTRODUCTION

The electrical excitability of nerve and muscle tissue is strongly dependent upon the availability of voltage-gated sodium channels. The available pool of functional sodium channels is regulated in a time- and voltage-dependent manner by two pharmacologically, molecularly, and kinetically distinct processes of inactivation: fast inactivation and slow inactivation (Ruff et al., 1988; Ruben et al., 1992; Valenzuela and Bennett, 1994; Featherstone et al., 1996; Vedantham and Cannon, 1998). Fast sodium channel inactivation is characterized by rapid (millisecond time-scale) onset and recovery, leading to changes in the available pool of sodium channels over the time course of a single action potential. Onset and recovery of slow inactivation, however, require several seconds (Ruff et al., 1988; Featherstone et al., 1996; Wang and Wang, 1997). Slow sodium channel inactivation is therefore probably relevant only in cases of sustained or repetitive depolarization, where it would serve as a slow negative feedback on membrane excitability. In neurons, for example, accumulation of sodium channel slow inactivation has been shown to contribute to slow spike adaptation and action potential burst termination (Fleidervish et al., 1996). In skeletal muscle, differences in sodium channel slow inactivation may underlie differences in fast- and slow-twitch muscle excitability (Ruff et al., 1987).

Slow inactivation in voltage-gated cardiac sodium channels has not been thoroughly characterized, and the molecular basis for slow inactivation in any sodium channel is unknown. In the heart, sustained (several hundred milliseconds) and repetitive ($>$1 Hz) depolarization is a normal characteristic of cardiac myocyte function (Ganong, 1995). Under such conditions, nerve and skeletal muscle sodium channels would undergo almost complete slow inactivation within a few minutes. Because cardiac muscle remains excitable during sustained firing, we postulate that slow inactivation must differ substantially from that of nerve and skeletal muscle.

In this study, we pursued a complete biophysical characterization of cardiac muscle sodium channel (hH1a) inactivation. Here we show that slow inactivation in cardiac sodium channels is dramatically limited compared to slow inactivation in nerve and skeletal muscle. This alteration is a previously unrecognized, physiologically important difference between cardiac sodium channels and other sodium channel subtypes. The alteration in cardiac sodium channel slow inactivation may arise from the inhibition of slow inactivation by fast inactivation, because modification of fast inactivation by mutagenesis results in cardiac sodium channel slow inactivation that is faster and more complete.

## MATERIALS AND METHODS

cDNAs for the WT human heart sodium channel $\alpha$-subunit (hH1a) and fast inactivation modified mutant (hH1a IFM1488QQQ) were created as described (Hartmann et al., 1994). The $\beta_1$-subunit was a gift of the laboratory of L. Isom (Isom et al., 1992). For each clone, 1 $\mu$g of linearized template was used to perform in vitro transcriptions using mMessage mMachine kits from Ambion (Austin, TX), using T7 polymerase for hH1a WT and mutant, and T3 polymerase for the $\beta$-subunit. RNA for injection was precipitated and resuspended in 1 mM Tris-Cl (pH 6.5) at a concentration of ~1 mg/ml.

*Received for publication 15 December 1997 and in final form 17 March 1998.*

Address reprint requests to Dr. Peter C. Ruben, Department of Biology, Utah State University, Logan, UT 84322-5305. Tel.: 435-797-2490; Fax: 435-797-1575; E-mail: pruben@cc.usu.edu.

Dr. Richmond's present address is Department of Biology, University of Utah, Salt Lake City, UT 84112.

Dr. Feathersone's present address is Department of Biology, University of Utah, Salt Lake City, UT 84112.

Dr. Hartmann's present address is Department of Molecular Physiology/Biophysics, Baylor College of Medicine, Houston, TX 77030.



0006-3495/98/06/2945/08 $2.00

Stage V-VI oocytes were surgically removed from female *Xenopus laevis* (Nasco, Modesto, CA) anesthetized with 0.17% tricaine methanesulfonate (Sigma, St. Louis, MO). After surgery, frogs recovered in isolation in a shallow tank of distilled water. After full recovery, frogs were returned to the large rearing tank. Frogs routinely undergo up to six surgeries (at a frequency of less than one surgery every 2 months) with no obvious ill effects. After six surgeries, frogs are anesthetized and sacrificed by freezing under anesthesia, in accordance with institutional guidelines.

Theca and follicle cells were enzymatically removed from the oocytes by gently agitating the oocytes in a solution containing (in mM) 96 NaCl, 2 KCl, 1 $MgCl_2$, 5 HEPES (pH 7.4), with 2 mg/ml collagenase (Sigma) for ~1 h. After enzymatic treatment, oocytes were rinsed several times in a solution containing (in mM) 96 NaCl, 2 KCl, 1 $MgCl_2$, 5 HEPES (pH 7.4), then placed in sterile incubation medium containing (in mM) 96 NaCl, 2 KCl, 1 $MgCl_2$, 1.8 $CaCl_2$, 5 HEPES, 2.5 pyruvic acid (pH 7.4), with 1–5% horse serum (Irvine Scientific, Irvine, CA) and gentamycin sulfate 100 mg/liter, at 18°C. Approximately 24 h after enzymatic treatment, oocytes were individually injected with 25 nl of mRNA, using a Drummond automatic injector, and then further incubated in 60-mm disposable petri dishes with gentle agitation (~60 rpm on a small rotary shaker) at 18°C until electrophysiological recording 3–14 days later. The incubation solution bathing the oocytes was changed daily. For almost all experiments, only $\alpha$-subunit RNA was injected, based on the inconclusive evidence that cardiac sodium channels are coassociated with $\beta_1$-subunits in vivo (Fozzard and Hanck, 1996), and on our observations that coexpression of the $\alpha$- and $\beta_1$-subunits did not affect slow inactivation or test pulse fast inactivation (data not shown). In the experiment in which we tested the effect of $\beta_1$-subunit on steady-state slow inactivation, $\alpha$- and $\beta_1$-subunits were coinjected as a 1:1 volume mixture. Because of the much smaller size of the $\beta_1$-subunit and more efficient translation, this probably provides a saturating concentration of $\beta_1$-subunit protein.

In preparation for macropatch recording, the vitelline membrane was manually removed from oocytes after a short (2–5 min) exposure to a hyperosmotic solution containing (in mM) 96 NaCl, 2 KCl, 20 $MgCl_2$, 5 HEPES, 400 mannitol (pH 7.4). All macropatch recording was done using a bath solution predicted to be isopotential and isosmolar with the intracellular oocyte milieu and containing (in mM) 9.6 NaCl, 88 KCl, 11 EGTA, 5 HEPES (pH 7.4). Aluminosilicate patch electrodes were pulled on a Sutter P-87 pipette puller, dipped in melted dental wax to reduce capacitance, fire polished, and filled with (in mM) 96 NaCl, 4 KCl, 1 $MgCl_2$, 1.8 $CaCl_2$, 5 HEPES (pH 7.4).

Electrophysiological recordings were made using an EPC-9 patch-clamp amplifier (HEKA, Lambrecht, Germany), and digitized at 5 kHz via an ITC-16 interface (Instrutech, Great Neck, NY). Voltage clamping and data acquisition were controlled via Pulse software (HEKA) running on a Power Macintosh 7100/80. All data were low-pass-filtered at 5 kHz during acquisition. The experimental bath temperature was maintained at 22 ± 0.2°C for all experiments by using a Peltier device controlled by an HCC-100A temperature controller (Dagan, Minneapolis, MN). After seal formation, patches were left on-cell for all recordings. On-cell patches were more stable, allowing long-term recordings, and, because of the predicted similar cytosolic and extracellular $[K^+]$, showed no differences in sodium currents or voltage dependence compared to excised inside-out patches.

Because the study of slow inactivation required long recording durations and extended bouts of pulsing, we were very careful to avoid time- and pulsing-related artifacts, which add anomalous time constants to inactivation and recovery. When the voltage dependence of inactivation was studied, the clamp control software (Pulse) alternated prepulse potentials, such that prepulse potentials were delivered as −160 mV, +10 mV, −155 mV, +5 mV, −150 mV, etc. over the voltage range of −160 mV to +10 mV in 5-mV steps. Time-related distortions of steady-state slow inactivation curves were further avoided by gathering data by two prepulse protocols: first the membrane was stepped to all "even" voltages (e.g., −160, 0, −140, −20 mV, etc.), followed next by "odd" voltages (e.g., −150, −10, −130, −30 mV, etc.). Before every slow inactivation prepulse, we always allowed 30 s at −150 mV to ensure complete recovery from all inactivation and to avoid any accumulation of inactivation throughout the experiment. Prepulses were 500 ms long for steady-state fast inactivation, and 1 min for steady-state slow inactivation.

The holding potential for all experiments was −120 mV to −150 mV. Leak subtraction was performed automatically by the software by a p/4 protocol. Leak pulses alternated in direction from a holding potential of −120 mV. Leak pulses were always performed after the test pulse, and sufficient time between protocols was allowed to ensure that the leak pulses would have no effect on the data.

Subsequent analysis and graphing were done using Pulsefit (HEKA) and Igor Pro (Wavemetrics, Lake Oswego, OR), both run on a Power Macintosh 7100/80. Conductance (voltage) curves were computed using the equation

$$G = I_{max}/(V_m - E_{rev}) \tag{1}$$

where $G$ is conductance, $I_{max}$ represents the peak test pulse current, $V_m$ is the test pulse voltage, and $E_{rev}$ is the measured reversal potential. Steady-state activation and fast inactivation were fit by a Boltzmann distribution, as follows:

$$\text{Normalized current amplitude} = 1/1 + \exp(-ze_0(V_m - V_{1/2})kT)) \tag{2}$$

where "normalized current amplitude" is measured during a variable-voltage test pulse from a holding potential of −150 mV (for steady-state activation) or during a test pulse to 0 mV after a variable-voltage prepulse (for steady-state inactivation). $z$ is apparent valence, $e_0$ is the elementary charge, $V_m$ is the test pulse/prepulse potential, $V_{1/2}$ is the midpoint voltage, $k$ is the Boltzmann constant, and $T$ is absolute temperature. Descriptions of test pulse inactivation rates, given as time constants ($\tau$), were derived from fitting the monoexponential decay of individual currents according to the function

$$I(t) = I_{SS} + a_1 \exp(-t/\tau) \tag{3}$$

where $I(t)$ is the current amplitude as a function of time, $I_{ss}$ is the steady-state current, or asymptote (plateau amplitude), $a_1$ is the amplitude at time = 0 (time of peak current), and $\tau$ is the time constant (in ms). Time constants for the onset (and recovery) of inactivation were measured in the same way, except that fits were to peak current amplitude versus prepulse (or interpulse) duration. Descriptions of first-order, two-state reaction kinetics were derived by fitting $\tau$ versus voltage curves according to the following equation:

$$\tau(V_m) = 1/(k_f + k_b) \tag{4}$$

where $\tau(V_m)$ represents the time constant of progression to equilibrium as a function of membrane potential; $k_f$ is the rate of the forward reaction (not inactivated → inactivated), and $k_b$ is the rate of the backward reaction (inactivated → not inactivated), and were determined as follows:

$$k_f = A \exp + ((z(1 - \delta)(V_m - V_{1/2}))/kT) \tag{5}$$

$$k_b = A \exp - ((z\delta(V_m - V_{1/2}))/kT) \tag{6}$$

where $A$ = 1/2 rate at $V_0$, $z$ = total reaction valence (in electronic charge); $\delta$ = fractional barrier distance; $V_m$ = membrane potential (in mV); $V_{1/2}$ = midpoint potential (in mV). Steady-state probability was predicted using

$$p(t\infty) = k_f/(k_f + k_b) \tag{7}$$

where $p(t\infty)$ represents the probability of being inactivated at equilibrium.

$N$, throughout the text, refers to the number of experiments. All statistically derived values, both in the text and in figures, are given as mean ± standard error (SEM). Although only a single fit to averaged data is presented in Figs. 2 and 3, fits were performed for each data set to obtain SEM values for the time constants and steady-state availability. Results obtained by the two methods were not significantly different.

## RESULTS

Several days after RNA injection, two-electrode whole-cell voltage clamping of injected oocytes showed large (5–20 $\mu$A) sodium currents. Oocytes expressing the largest currents were then manually devitellinized and studied by patch-clamp techniques. All data were obtained from macropatches, which allowed excellent voltage control and yielded data that closely match results from cardiac channels in native tissue (Schneider et al., 1994) or heterologously expressed in mammalian cells (Wang et al., 1996).

In Fig. 1 *A*, a typical family of cardiac WT test pulse currents to different voltages is shown. Fast inactivation in these test pulses was always fast and monoexponential, despite lack of coinjected $\beta_1$-subunit, consistent with the finding that cardiac voltage-gated sodium channels in vivo do not require $\beta$-subunits for normal inactivation (see discussion in Fozzard and Hanck, 1996). As in skeletal muscle (Featherstone et al., 1996) and brain sodium channels (West et al., 1992), fast inactivation was modified by mutation of the three amino acids IFM to QQQ in the domain III-IV linker (Hartmann et al., 1994). A family of typical test pulse currents in the cardiac IFM mutant is shown in Fig. 1 *B*. The voltage dependence of activation in both the cardiac WT and IFM mutant was not different, as shown by the overlapping conductance curves in Fig. 1 *C*. To ensure that all channels were available for activation, the holding potential for all activation measurements was −150 mV. Note that conductance in both WT and IFM mutant saturates at approximately −20 mV. Test pulses to 0 mV were used in all subsequent experiments, except those for Fig. 3, which used a test pulse to −20 mV.

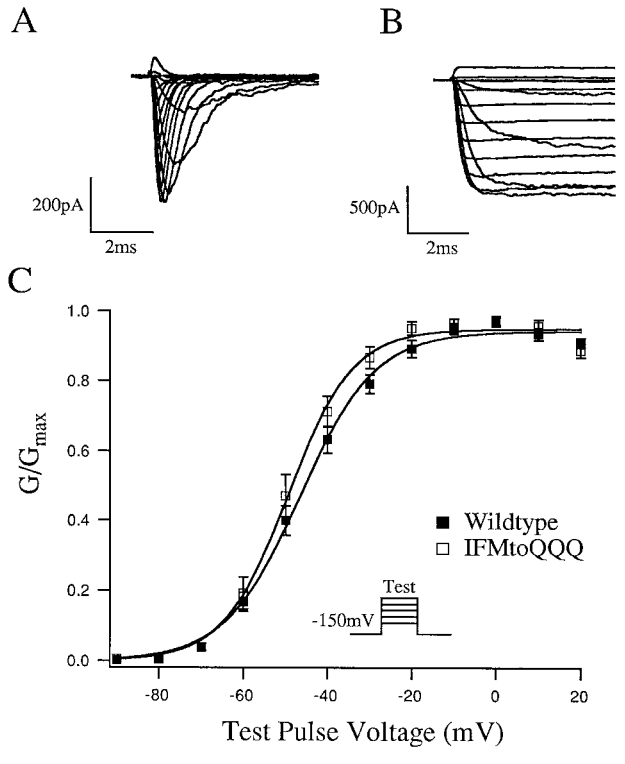


FIGURE 1 Activation in wild-type (hH1a WT) and fast-inactivation-modified mutant (hH1a IFM1488QQQ) human cardiac muscle sodium channels. Typical macropatch sodium currents are shown in response to a series of test pulses (−90 mV to +20 mV) from a $V_{hold}$ of −150 mV, for WT (Fig. 1 *A*) and IFM1488QQQ (Fig. 1 *B*) sodium channels. Fig. 1 *C* shows normalized, mean ± SEM conductance for WT (■) and IFM1488QQQ (□) channels. Solid lines show Boltzmann fits to the averaged data, which yield the following coefficients: $z$ = 2.89$e$ (WT), 3.36$e$ (IFM1488QQQ); $V_{1/2}$ = −47 mV (WT), −49 mV (IFM1488QQQ). $N$ = 12 (WT), 9 (IFM1488QQQ).

In previous work (Featherstone et al., 1996; Richmond et al., 1997) we found that a detailed understanding of fast inactivation kinetics was required to ensure proper isolation and characterization of slow inactivation. Therefore, we first characterized the voltage dependence and kinetics of fast inactivation, as shown in Fig. 2.

The kinetics of recovery from fast inactivation were measured by fast inactivating all channels with a prepulse to 0 mV for 500 ms, then stepping to an "interpulse" recovery voltage, during which channels began to recover from inactivation. After the interpulse, channel availability was assayed by a test pulse to 0 mV (see protocol diagram in Fig. 2 *A*). Test pulse amplitude after recovery was normalized to the current amplitude after a holding potential of −150 mV, where all channels should be available (not inactivated). As shown in Fig. 2 *A*, the fraction of channels that recovered from fast inactivation increased with increasing interpulse duration. Furthermore, both the rate of recovery and steady-state fraction recovered increased at more negative interpulse voltages. Recovery rate (given as a time constant) and steady-state recovered fraction (given as an asymptote) were quantified by fitting single exponential curves to data in Fig. 2 *A*.

Fast inactivation onset was studied by measuring the test pulse current amplitude after a prepulse of defined duration and voltage (see protocol diagram in Fig. 2 *B*). As shown in Fig. 2 *B*, the fraction of inactivated channels increased as prepulse duration increased. The rate of inactivation and steady-state fraction of inactivated channels also increased at more positive prepulse voltages. Inactivation onset and steady-state inactivation were quantified by fitting single exponential curves to the data in Fig. 2 *B*.

In Fig. 2 *C*, time constants from fits to fast inactivation onset and recovery data (*circles* and *squares*, respectively) such as those shown in Fig. 2, *A* and *B*, are plotted against membrane (interpulse or prepulse) potential. Also included in this figure (*triangles*) are time constants derived from single exponential fits to the decay of test pulse currents such as those shown in Fig. 1 *A*. Time constants of test pulse decay are referred to here as "open state fast inactivation," to differentiate them from inactivation time constants obtained at voltages where fast inactivation occurs without channel opening (Goldman, 1995), which we refer to as "closed state fast inactivation." As in skeletal muscle sodium channels (Featherstone et al., 1996), the averaged time constants in Fig. 2 *C* were well fit by a two-state (not inactivated → inactivated) first-order reaction model (see Materials and Methods). The coefficients of this fit suggest

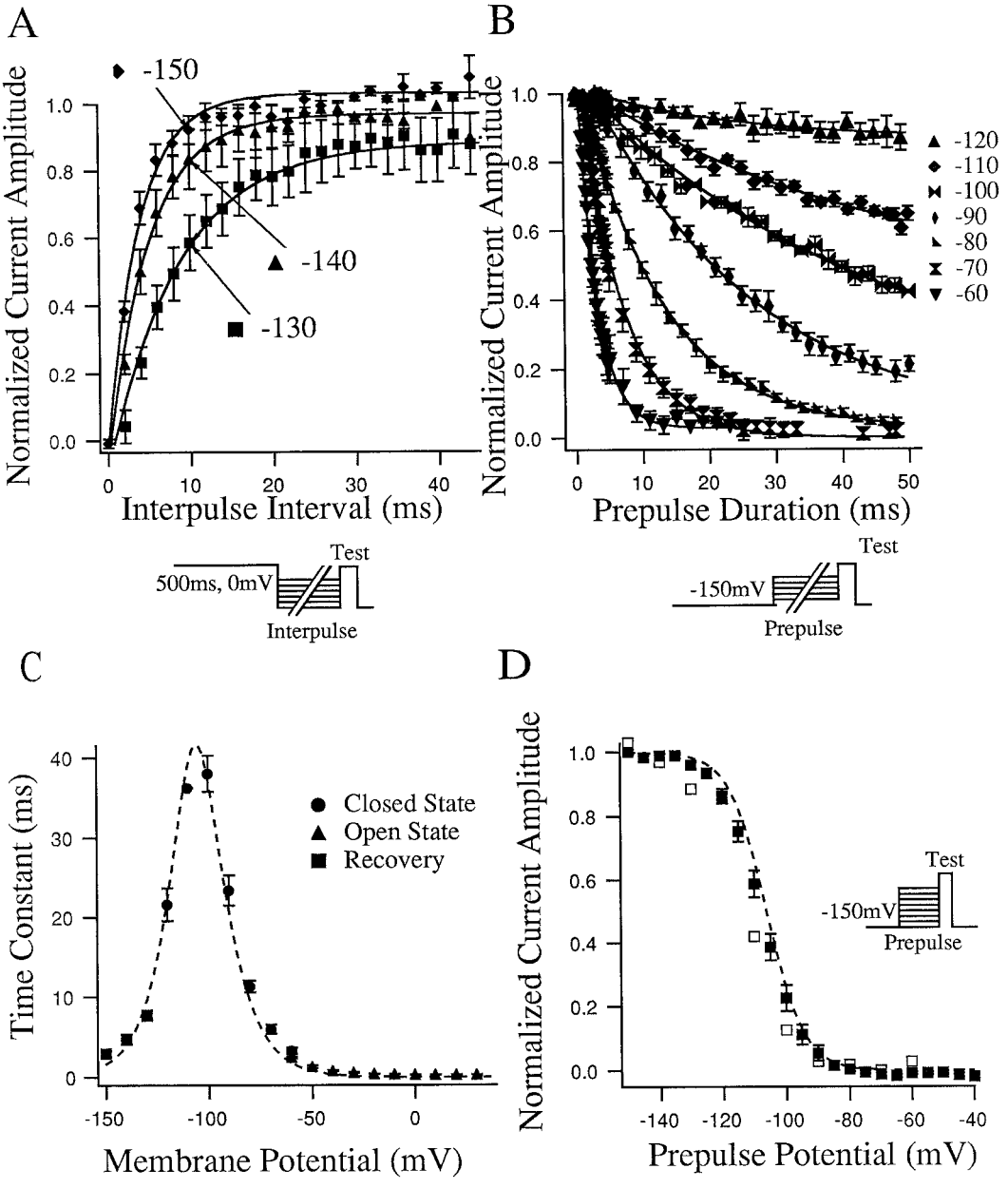


FIGURE 2 Fast inactivation in WT cardiac muscle sodium channels. (*A*) The average, normalized fast recovery of sodium current versus time (*N* ranged from 5 to 17). (*B*) Fast inactivation of sodium current versus time (*N* ranged from 5 to 9). In both *A* and *B*, solid lines are single exponential fits. Time constants from single exponential fits to data such as those shown in *A* and *B* are plotted versus voltage in *C*, where squares represent time constants of recovery (as in *A*), circles represent closed state fast inactivation (as in *B*), and triangles represent time constants of open state fast inactivation, from single exponential fits to decay of test pulses, such as those shown in Fig. 1 *A*. (*D*) Steady-state fast inactivation after 500-ms prepulses (■, $N = 25$), and asymptotes (□) from single exponential fits to averaged data shown in *B*. The dashed lines in *C* and *D* are predictions of a first-order reaction model (not inactivated → inactivated) with the following coefficients: $\tau_{max} = 41.6$ ms; reaction valence = 4.3*e*; $V_{1/2} = -106$ mV. All values represent mean ± SEM.

a maximum time constant of 41.6 ms, a total reaction valence of 4.3*e*, a relative barrier position of 0.51, and a reaction midpoint of −106 mV. Fig. 2 *D* shows that this model, using the same coefficients, also provides (*dashed line*) a very good prediction of steady-state fast inactivation, when steady-state values are measured after 500-ms prepulses. The steady-state inactivation values in Fig. 2 *D* are also matched closely by the asymptotes of exponential fits to the data in Fig. 2, *A* and *B*.

When depolarized to positive potentials for long periods of time, sodium channels enter a state of inactivation from which recovery takes several seconds. Because entry into this second state of inactivation takes relatively long depolarizations and recovers slowly, this process has been called "slow inactivation" (Rudy, 1978, 1981). Fig. 3 shows results of experiments designed to characterize the kinetics of slow inactivation in both WT and IFM-QQQ mutant cardiac sodium channels. The IFM-QQQ mutation is presumed to

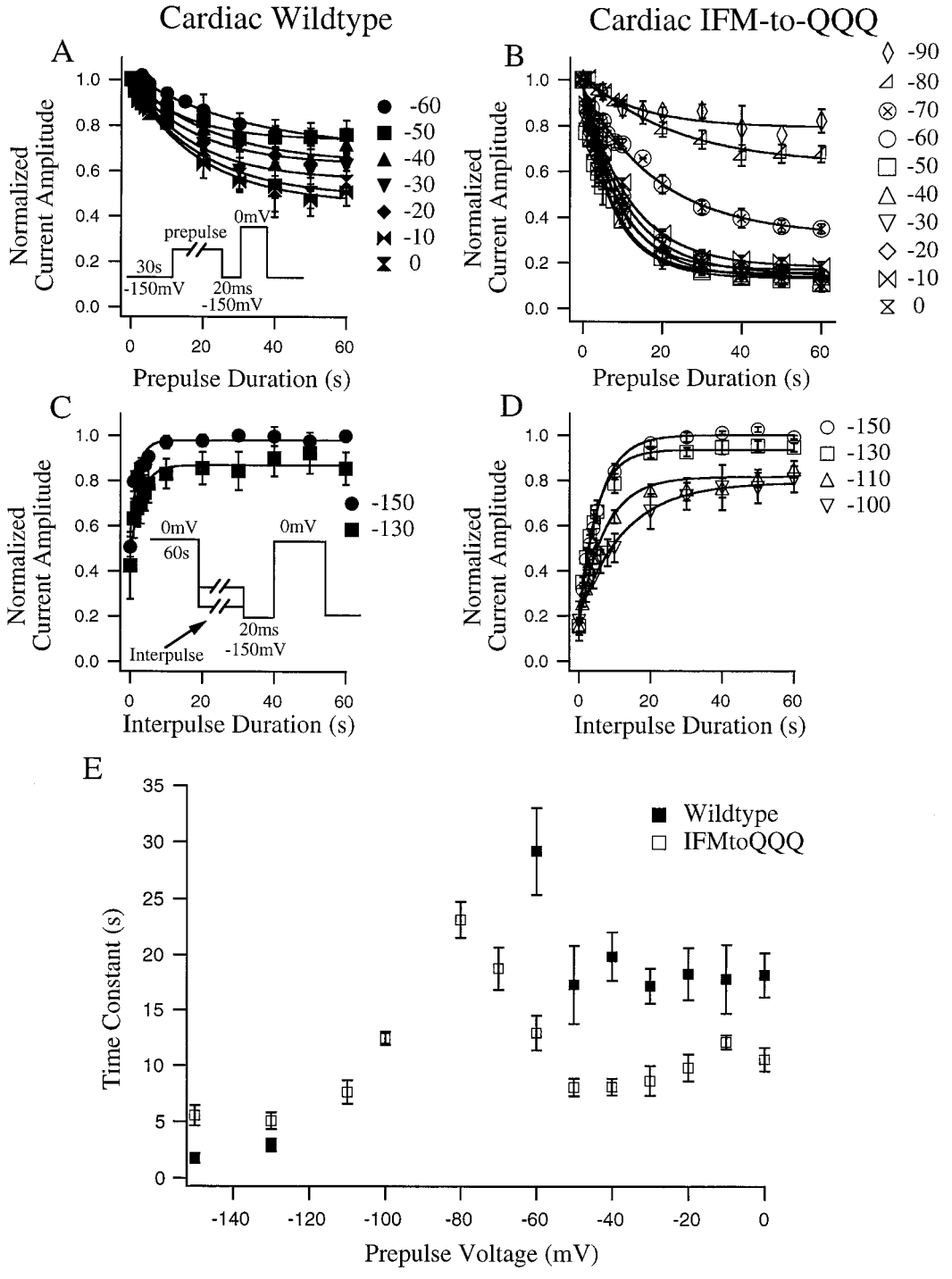


FIGURE 3 Kinetics of slow inactivation in WT and IFM1488QQQ cardiac sodium channels. (*A* and *B*) Onset of slow inactivation for WT (*N* ranged from 4 to 11) and IFM1488QQQ (*N* ranged from 3 to 12) cardiac sodium currents, respectively. The average, normalized currents obtained at 0 mV after a prepulse of increasing duration over a range of potentials (−90 mV to 0 mV) are plotted against prepulse duration and fit with a single exponential. (*C* and *D*) Recovery rates of slow inactivation for WT (*N* ranged from 3 to 8) and IFM1488QQQ (*N* ranged from 3 to 6) cardiac sodium currents after a 60-s conditioning pulse at 0 mV to fully slow inactivate the channels. Average, normalized currents obtained at 0 mV are plotted against interpulse duration for the voltages displayed and fit with a single exponential. (*E*) Average time constants for slow inactivation in WT, derived from single exponential fits to all of the data shown in *A–D*. Increasing the number of exponentials did not improve the fit. All values represent mean ± SEM.

modify fast inactivation by removing the pore-blocking particle (West et al., 1992). In general, the approach used for Fig. 3 is similar to that used for characterizing fast inactivation in Fig. 2 (see protocol diagrams in each figure), except

1. A 1-min prepulse to 0 mV was used to slow inactivate channels (rather than a 500-ms prepulse to 0 mV).

2. A 20-ms fast inactivation recovery pulse to −150 mV was used to selectively recover fast inactivated channels

before the test pulse (see pulse protocol *inset*, Fig. 3 *A*) or after the recovery pulse (see pulse protocol *inset*, Fig. 3 *C*), so that onset or recovery of only slow inactivation was measured. As seen in Figs. 2 *C* and 3, 20 ms at −150 ms completely recovers fast inactivation, but no measurable amount of slow inactivation.

3. The membrane was stepped to −150 mV for 30 s before every prepulse to ensure that accumulation of inactivation (or recovery) did not occur during the experiment and thus distort our kinetic measurements.

Like fast inactivation, slow inactivation in both WT and IFM mutant cardiac channels occurs more quickly and completely at depolarized potentials (Fig. 3, *A* and *B*), and recovery from slow inactivation occurs more quickly and completely at hyperpolarized potentials (Fig. 3, *C* and *D*). Onset and recovery of slow inactivation in both WT and IFM mutant cardiac channels were best fit with a single exponential; the time constants are plotted in Fig. 3 *E*. No wild-type slow inactivation recovery is shown at −100 to −120 mV because, as seen in Fig. 2 *D*, sufficient fast inactivation accumulates at these voltages to distort measures of slow inactivation recovery. Because fast inactivation is removed by the IFM-QQQ mutation, recovery measurements are possible at all voltages. As in skeletal muscle sodium channels (Featherstone et al., 1996), time constants reached an apparent plateau at potentials more positive than about −40 mV, and time constants for slow inactivation in IFM mutant channels were significantly faster than those of WT.

Steady-state slow inactivation for WT and IFM mutant cardiac channels is plotted in Fig. 4 *C*. Steady-state slow inactivation was measured by using a 60-s prepulse, followed by a 20-ms, −150 mV fast inactivation recovery pulse immediately before the 0-mV test pulse. As in Fig. 3, a step to −150 mV for 30 s occurred before every prepulse, to cause channels to completely recover from all inactivation and avoid artifacts due to accumulation of slow inactivation. As an additional precaution against artifacts, prepulse voltages were alternated between highest and lowest voltages, and the entire curve was collected in two parts (see Materials and Methods for more detail). After 60 s at +10 mV, a large percentage of current in WT channels is not affected by slow inactivation (Fig. 4 *A*), whereas almost all of the current slow inactivated in IFM mutant channels (Fig. 4 *B*). As seen in Fig. 4 *C*, over half of WT cardiac channels failed to slow inactivate, even at positive potentials, whereas IFM mutant cardiac channels were almost fully slow inactivated by about −50 mV.

To verify that the low percentage of slow inactivated WT cardiac sodium channels was not due to an insufficiently long prepulse, slow inactivation was compared after pre-

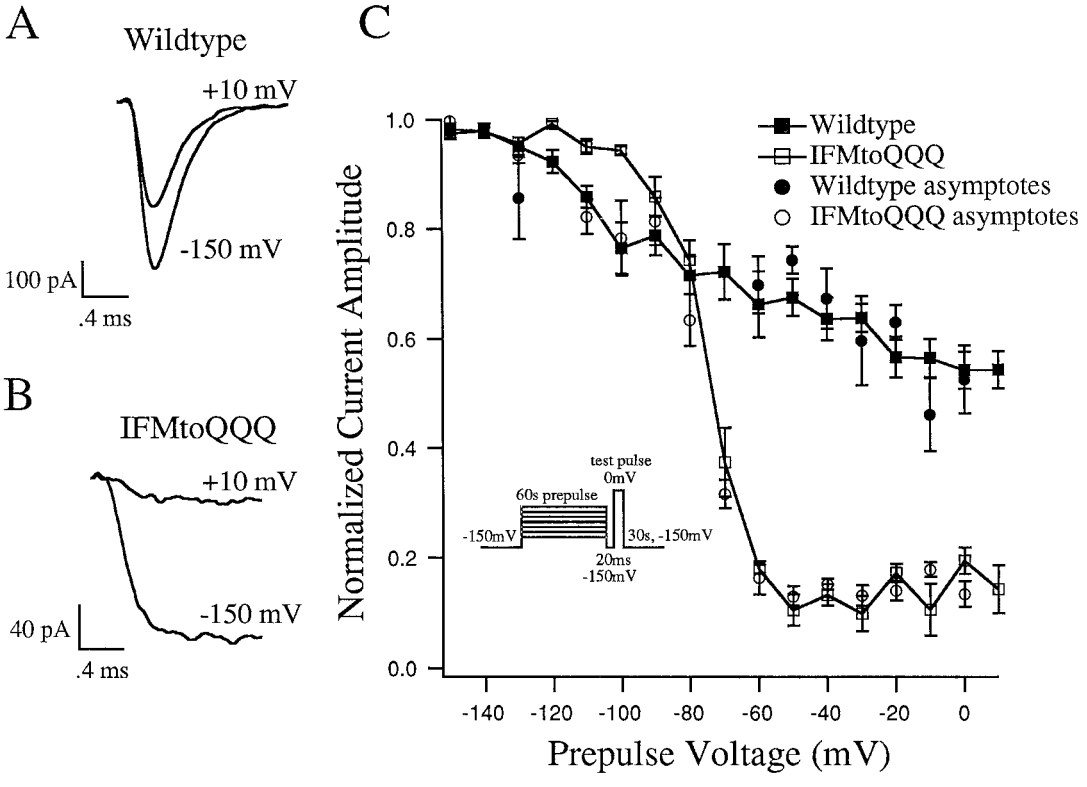


FIGURE 4 Steady state slow inactivation in WT and IFM1488QQQ cardiac sodium channels. (*A* and *B*) Typical traces obtained after a 60-s prepulse to −150 mV and +10 mV, for WT and IFM1488QQQ cardiac sodium currents, respectively. In *C* the steady-state slow inactivation of WT ($N = 11$) and IFM1488QQQ ($N = 16$) sodium currents is plotted as average normalized current amplitude versus 60-s prepulse voltage (■, □). Added to *C* are the asymptotes (●, ○, mean ± SEM) derived from exponential fits to the onset of slow inactivation curves at each voltage tested (summarized in Fig. 3, *A* and *B*).

pulses of 1 min and 2 min in a separate experiment ($N = 3$, data not shown). For this experiment, current amplitude was first measured during a test pulse to 0 mV, from a holding potential of −150 mV. Next, the channels were clamped at +10 mV for 1 min, and channel availability was assayed with a 0-mV test pulse after a 20-ms, −150-mV fast inactivation recovery pulse. Channels were then fully recovered from all inactivation (via a step to −150 mV for 30 s), held at +10 mV for 2 min, assayed, then recovered and assayed again as a check against rundown or other artifacts. One-minute prepulses left 71 ± 7% of the WT current unaffected by slow inactivation, consistent with Fig. 4 *C*. Two-minute prepulses left 69 ± 6% of the WT current unaffected by slow inactivation (not a statistically significant difference; $p = 0.8$). As an additional check, Fig. 4 *C* includes asymptotes derived from monoexponential fits to slow inactivation onset data such as those shown in Fig. 3, *A* and *B*. These asymptotes agree well with the 1-min prepulse slow inactivation data for both WT and the IFM mutant, further suggesting that steady state was achieved, and no slower components of slow inactivation were missed.

In Fig. 5, slow inactivation is compared between hH1a and hSkM1 channel isoforms, using the same protocol to assay slow inactivation as described for Fig. 4 *C*. As we have previously demonstrated (Featherstone et al., 1996), ~20% of skeletal muscle sodium channels do not completely inactivate after 1-min depolarizations. Fig. 5 demonstrates, however, that cardiac sodium channels (same data as shown in Fig. 4 *C*, $N = 7–9$) slow inactivate even less completely than do skeletal muscle sodium channels ($N = 17–19$).

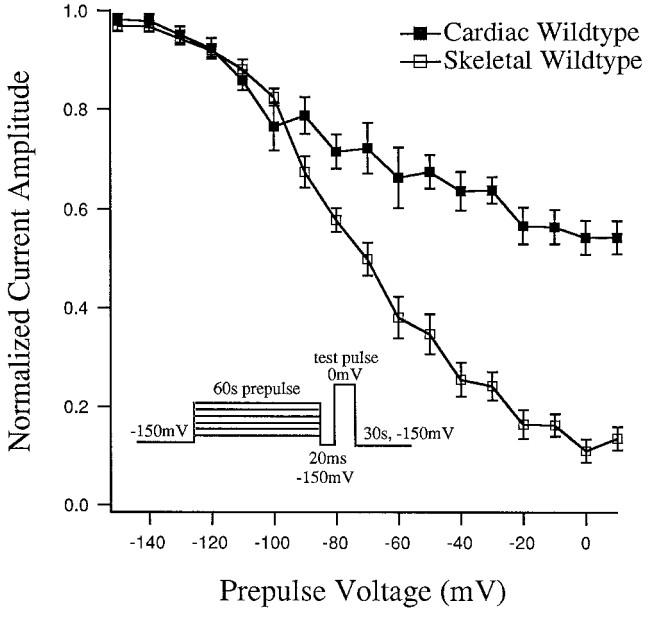


FIGURE 5 Steady-state slow inactivation in hSkM1 and hH1a sodium channels. Normalized average current amplitudes (± SEM) for WT cardiac channel s (■, $N = 11$) and WT skeletal muscle channels (□, $N = 17–19$) are plotted as a function of 60-s prepulse voltages.

## DISCUSSION

The goal of this study was to characterize slow inactivation in cardiac muscle (hH1a) sodium channels. Comparisons between cardiac sodium channels and other sodium channel subtypes are interesting because of the dramatic differences in typical action potential time course between cardiac and other tissues (e.g., skeletal muscle, nerve). Previous work (Featherstone et al., 1996; Richmond et al., 1997; Hayward et al., 1997), for example, suggests that the long-duration (several hundred ms), repetitive action potentials in functioning cardiac myocytes would soon slow inactivate skeletal muscle sodium channels. We therefore predicted that cardiac sodium channel slow inactivation must differ in some fundamental way from that of skeletal muscle sodium channels. Indeed, we found that only ~20% of WT cardiac sodium channels are slow inactivated at steady state, compared to 80% of skeletal muscle sodium channels (Featherstone et al., 1996). Because the molecular underpinnings of slow inactivation are still unknown, this information may not only be important for an understanding of normal muscle membrane physiology, but may also help to clarify structure/function relationships in sodium channels.

To help ensure accurate identification of slow inactivation, we first characterized the voltage dependence and kinetics of fast inactivation and confirmed its identity at all voltages using the IFM to QQQ mutation, which is presumed to remove the blockade of the channel pore by the putative fast inactivation particle (West et al., 1992). In this way, we were able to account for and identify two inactivation processes: fast inactivation and slow inactivation. Both the time course and voltage dependence of our fast inactivation measurements are similar to patch-clamp results from native sodium channels in ventricular myocytes (Brown et al., 1981; Shander et al., 1995; Ono et al., 1993) and Purkinje cells (Hanck and Sheets, 1995). Fast and slow inactivation processes have also been identified in rat ventricular myocytes (Shander et al., 1995). These previous data, although limited to recovery at −30 mV, support our conclusion that only ~20% of WT cardiac channels slow inactivate. Despite the similarities between our findings and previous studies in native channels, it is possible that the *Xenopus* expression system could result in altered voltage sensitivity of the fast and slow inactivation processes. It is also possible that the 500-ms prepulse duration used to determine the steady-state distribution of fast inactivated channels could slightly exaggerate the curve's steepness, because a few channels might have slow inactivated during the prepulse.

As in skeletal muscle sodium channels (Featherstone et al., 1996), modification of fast inactivation by the IFM-QQQ mutation resulted in slow inactivation that was faster (Fig. 3) and more complete (Fig. 4). Partial modification of fast inactivation by the F→Q mutation also makes slow inactivation more complete (Townsend and Horn, 1997). We have previously hypothesized (Featherstone et al., 1996) that fast inactivation might limit the extent of slow inactivation via charge immobilization (Armstrong and

Bezanilla, 1977). Hence, if slow inactivation is dependent on charge (i.e., S4 mobility), then charge immobilization due to fast inactivation might limit this mobility and, thus, limit slow inactivation. Our present data are consistent with this idea. If this idea is true, then differences in sodium channel slow inactivation between cardiac muscle and skeletal muscle (Fig. 5) suggest that S4 mobility could be restricted to a greater extent in hH1a channels, a hypothesis that could be tested using gating current measurements. If slow inactivation is limited by fast inactivation-induced charge immobilization, then experiments comparing charge immobilization in hH1a and hSkM1 should show greater charge immobilization in cardiac channels than in skeletal muscle channels. Because we have observed additional slow inactivation in IFM-QQQ mutants of both hH1a and hSkM1 (compared to wild-type channels), inhibition of slow inactivation by fast inactivation may be a general characteristic of voltage-gated sodium channels. The greater inhibition of slow inactivation in hH1a, however, may be an adaptation to ensure continued sodium channel availability despite the prolonged depolarizations that occur during normal cardiac muscle function.

Several point mutations have been identified in rat SkM1 sodium channels that affect slow inactivation: T698M (Cummins and Sigworth, 1996), M1585V (Hayward et al., 1997), and N434A (Wang and Wang, 1997). The mutations T698M, M1585V, and N434A, as well as the WT cardiac channels studied here, show differences in steady-state slow inactivation when compared to WT rSkM1 sodium channels. T698M, M1585, and N434, however, are all conserved between skeletal and cardiac muscle sodium channels (Kallen et al., 1990). Therefore, other differences between hH1a and skeletal muscle sodium channels must explain the lack of slow inactivation in cardiac channels. Future experiments with hH1a-hSkM1 chimeras may allow identification of the structure(s) mediating the putative interaction between fast and slow inactivation.

We thank Clay Prince and Jonathan Olsen for assistance with oocyte injection and care, and Esther Fujimoto for RNA preparation.

This work was supported by Public Health Service grant R-01 NS29204 to PCR and an American Heart Association, Utah Affiliate, grant-in-aid to JER and PCR.

## REFERENCES

Armstrong, C. M., and F. Bezanilla. 1977. Inactivation of the sodium channel. II. Gating current experiments. *J. Gen. Physiol.* 70:567–590.

Brown, A. M., K. S. Lee, and T. Powell. 1981. Sodium current in single rat heart muscle cells. *J. Physiol. (Lond.).* 318:479–500.

Cummins, T. R., and F. J. Sigworth. 1996. Impaired slow inactivation in mutant sodium channels. *Biophys. J.* 71:227–236.

Featherstone, D. E., J. E. Richmond, and P. C. Ruben. 1996. Interaction between fast and slow inactivation in Skm1 sodium channels. *Biophys. J.* 71:3098–3109.

Fleidervish, I. A., A. Freidman, and M. J. Gutnick. 1996. Slow inactivation of Na+ current and slow cumulative spike adaptation in mouse and guinea-pig neocortical neurones in slices. *J. Physiol. (Lond.).* 493.1:83–97.

Fozzard, H. A., and D. A. Hanck. 1996. Structure and function of voltage-dependent sodium channels: comparison of brain II and cardiac isoforms. *Physiol. Rev.* 76:887–926.

Ganong, W. F. 1995. Review of Medical Physiology. Appleton and Lang, Norwalk, CT.

Goldman, L. 1995. Sodium channel inactivation from closed states: evidence for an intrinsic voltage dependency. *Biophys. J.* 69:2369–2377.

Hanck, D. A., and M. F. Sheets. 1995. Modification of inactivation in cardiac sodium channels: ionic current studies with anthopleurin-A toxin. *J. Gen. Physiol.* 106:601–616.

Hartmann, H. A., A. A. Tiedman, S.-F. Chen, A. M. Brown, and G. E. Kirsch. 1994. Effects of III-IV linker mutations on human heart Na+ channel inactivation gating. *Circ. Res.* 75:114–122.

Hayward, L., R. Brown, and S. Cannon. 1997. Slow inactivation differs among mutant Na channels associated with myotonia and periodic paralysis. *Biophys. J.* 72:1204–1219.

Isom, L. L., K. S. D. Jongh, D. E. Patton, B. F. X. Reber, J. Offord, H. Charbonneau, K. Walsh, A. L. Goldin, and W. A. Catterall. 1992. Primary structure and functional expression of the B1 subunit of the rat brain sodium channel. *Science.* 256:839–842.

Kallen, R. G., Z.-H. Sheng, J. Yang, L. Chen, R. B. Rogart, and R. L. Barchi. 1990. Primary structure and expression of a sodium channel characteristic of denervated and immature rat skeletal muscle. *Neuron.* 4:233–242.

Ono, K., H. A. Fozzard, and D. A. Hanck. 1993. Mechanism of cAMP-dependent modulation of cardiac sodium channel current kinetics. *Circ. Res.* 72:807–815.

Richmond, J. E., D. E. Featherstone, and P. C. Ruben. 1997. Human $Na^+$ channels fast and slow inactivation in paramyotonia congenita mutants expressed in *Xenopus laevis* oocytes. *J. Physiol. (Lond.).* 499.3:589–600.

Ruben, P. C., J. G. Starkus, and M. D. Rayner. 1992. Steady-state availability of sodium channels. Interactions between activation and slow inactivation. *Biophys. J.* 61:941–955.

Rudy, B. 1978. Slow inactivation of the sodium conductance in squid giant axons. Pronase resistance. *J. Physiol. (Lond.).* 283:1–21.

Rudy, B. 1981. Slow inactivation of voltage-dependent channels. *In* Nerve Membrane: Biochemistry and Function of Channel Proteins. University of Tokyo Press, Tokyo, Japan. 89–111.

Ruff, R. L., L. Simoncini, and W. Stuhmer. 1987. Comparison between slow sodium channel inactivation in rat slow- and fast-twitch muscle. *J. Physiol. (Lond.).* 383:339–348.

Ruff, R., L. Simoncini, and W. Stuhmer. 1988. Slow sodium channel inactivation in mammalian muscle: a possible role in regulating excitability. *Muscle Nerve.* 11:502–510.

Schneider, M., T. Proebstle, V. Hannekum, and R. Rudel. 1994. Characterization of the sodium currents in isolated human cardiocytes. *Pflugers Arch.* 428:84–90.

Shander, G. S., Z. Fan, and J. C. Makielski. 1995. Slowly recovering cardiac sodium current in rat ventricular myocytes: effects of conditioning duration and recovery. *J. Cardiovasc. Electrophysiol.* 6:786–795.

Townsend, C., and R. Horn. 1997. Effect of alkali metal cations on slow inactivation of cardiac $Na^+$ channels. *J. Gen. Physiol.* 110:23–33.

Valenzuela, C., and J. P. B. Bennett. 1994. Gating of cardiac $Na^+$ channels in excised membrane patches after modification by a-chymotrypsin. *Biophys. J.* 67:161–171.

Vedantham, V., and S. C. Cannon. 1998. Slow inactivation does not affect movement of the fast inactivation gate in voltage-gated $Na^+$ channels. *J. Gen. Physiol.* 111:83–93.

Wang, D. W., J. A. L. George, and P. B. Bennett. 1996. Comparison of heterologously expressed human cardiac and skeletal muscle sodium channels. *Biophys. J.* 70:238–245.

Wang, S.-Y., and G. K. Wang. 1997. A mutation in segment I-S6 alters slow inactivation of sodium channels. *Biophys. J.* 72:1633–1640.

West, J. W., D. E. Patton, T. Scheuer, Y. Wang, A. L. Goldin, and W. A. Catterall. 1992. A cluster of hydrophobic amino acid residues required for fast $Na^+$-channel inactivation. *Proc. Natl. Acad. Sci. USA.* 89: 10910–10914.